Chemical Engineering Science 64 (2009) 5153–5161

Contents lists available at ScienceDirect

Chemical Engineering Science

journal homepage: www.elsevier.com/locate/ces

Flow and particle motion in scraped heat exchanger crystallizers

M. Rodriguez Pascual[a,*], J.J. Derksen[b], G.M. Van Rosmalen[a], G.J. Witkamp[a]

[a] Technical University Delft, The Netherlands
[b] University of Alberta, Canada

ARTICLE INFO

Article history:
Received 4 January 2009
Received in revised form 19 June 2009
Accepted 20 August 2009
Available online 1 September 2009

Keywords:
Fluid mechanics
Crystallization
Scaling
CFD
Lattice Boltzmann method
Scraped heat exchanger crystallizers
Chemical reactors

ABSTRACT

Turbulent fluid flow and related solid particle behaviour in the direct vicinity of the heat exchanging (HE) surface of a scraped heat exchanger crystallizer was studied. The liquid flow is visualized by dye injection and the particles are monitored directly for two types of commonly used scraper geometries. In conjunction with this experimental work, we performed direct numerical simulations of the two-phase (solid–liquid) flow system. Our main goal is the design of scraper geometries that enhance heat transfer by perturbing the thermal boundary layer, and effectively scrape off particles that nucleate, grow and adhere onto the HE surface. Also the turbulent flow generated by the moving scrapers should direct the particles into the bulk of the tank. The experiments and simulations show good qualitative resemblance which enables the design of scrapers based primarily on numerical predictions.

1. Introduction

The formation of an insulating scale layer on heat exchanger (HE) surfaces is a common problem in cooling and melt crystallization (Rao and Hartel, 2006; Pronk et al., 2008; Qin et al., 2006). The higher supersaturation close to the HE surface compared to the supersaturation in the bulk solution is the main cause of this phenomenon (Pronk et al., 2005). This higher supersaturation provokes higher nucleation and growth rates at the HE surface, and if no action is taken a scale layer of crystals is formed, that drastically decreases the heat transfer efficiency, and that can ultimately cause failure of the whole crystallization process (Vaessen et al., 2004).

Continuous scraping of the HE surfaces is commonly used to prevent scale formation. This mechanical action affects the fluid flow as well as the particle dynamics in the crystallizer by creating significant additional flow and turbulence. The influence of the scrapers on the flow dynamics not only depends on their position and velocity, but also on their particular shape. Therefore special attention has to be given to the geometry of the scraper. Although earlier studies have been done to visualize and to compute the flow on the scraper area (Yataghene et al., 2008; Duffy et al., 2007; Stranzinger et al., 2002; Fitt and Please, 2001), no experimental or computational studies of the particle trajectories have been done until now.

The scraper removes the fluid boundary layer at the HE surface, and turbulently mixes this fluid up with the bulk fluid, which increases heat transfer. Therefore the influence of the scrapers to the heat transfer on scraped heat exchangers has been extensively reported on literature (De Goede and De Jong, 1993; Vaessen et al., 2004; Landfeld et al., 2006). In some crystallizer designs no mixers are used, and the scrapers provide the only mechanical action that is responsible for the flow field and therefore for the temperature and particle distributions. Under conditions where the imposed heat flux causes a scale layer, stable operation is still feasible as long as the crystals formed closely above or on the HE surface are transported away from the surface. The scraper geometry should direct the particles into the bulk solution where they either dissolve or grow into the crystal size distribution. The role of the scraper geometry is therefore not limited to its effect on the flow but also determines the removal efficiency of the fluid boundary layer and the removal rate of the crystals from the surface.

In a former paper the turbulent flow at the bottom region between the scraper blades was obtained from large eddy simulations of a clear fluid. The simulated flow patterns could explain the difference in local heat transfer between the uniformly heated HE surface and the bulk solution (Rodriguez Pascual et al., 2009). In this paper we present a combined experimental and computational study of the fluid flow and particle dynamics closely above the HE surface of a crystallizer equipped with two commonly used scraper geometries.

Because visualization of particles and fluid flow during crystallization are very difficult to achieve; two different types of experiments were designed for either flow or particle visualization. The experimental results were compared with the results of direct numerical simulations (DNS) using the lattice-Boltzmann method. This experimental and computational study was focused on the

* Corresponding author.
E-mail address: M.RodriguezPascual@tudelft.nl (M.R. Pascual).

0009-2509/$ - see front matter © 2009 Elsevier Ltd. All rights reserved.
doi:10.1016/j.ces.2009.08.027

start-up behaviour of the flow-particle dynamics of the scraping area up to 300 s (corresponding to 350 scraper revolutions) after which the flow-particle conditions are more or less steady.

The aim of the work presented in this paper is in exploring the feasibility and potential of detailed numerical simulations for the design of scrapers. For this we focus on qualitatively correct predictions, and on the physical phenomena that need to be incorporated in the computational approach to get those. For instance, it appeared to be essential to incorporate particle–particle collisions in order to account for the build-up of particles in front of a scraper.

The paper is organized in the following manner: First we introduce the flow system and scraper geometries to be investigated; and we briefly describe the experimental setup for flow and particle visualization. Subsequently the essentials of the numerical method (lattice-Boltzmann discretization for the liquid flow, Lagrangian particle tracking for the solids) are given. In discussing the results, we consider the start-up and quasi-steady state behaviour of the two phase flow system by one-on-one comparing snapshots of computational and experimental results. The final section summarizes our main findings.

2. Experimental techniques

2.1. Apparatus

For experimental simplicity and because our research focussed on the scraper area, a laboratory scale scraped heat exchanger crystallizer designed for the formation of ice scaling from aqueous solutions was used. The crystallizer setup consists of a cylindrical 10 l transparent Plexiglas tank of 30 cm height and 20 cm diameter. On the centreline of the tank a vertical shaft is positioned connected to a rotor. The crystallizer has a 1 mm stainless steel bottom plate with a heat transfer area of 0.031 m^2, which is scraped by four rotating Teflon scraper blades of 99 mm length that are driven by the vertical shaft (Fig. 1). Two types of scrapers were used along with different holders. The flow in the tank was only driven by the motion of the scrapers; no additional impeller was installed.

The scraper in Fig. 2a has a vertical shape that ends in a sharp tip and is attached to the scraper arm by a top holder. A normal force to the heat exchanger plate is applied by springs or air pressure balloons that are located between the holder and the scraper. These kinds of scrapers are commonly used in different types of cooling crystallizers. Preliminary experiments had shown that the vertical shape of the scraper leads to a build-up of particles in front of the scraper. A second type of scraper as given in Fig. 2b was, therefore, designed with a more streamlined shape without exterior holders or other protrusions. The scrapers are attached to the shaft by an interior metal bar, and the force exerted on the heat exchanger surface is applied by torsion of this bar.

2.2. Flow visualization

The flow around the scrapers was visualized by releasing a coloured dye. The schematic experimental setup is shown in Fig. 3. A 1% potassium permanganate water solution, with a strong purple colour was injected at three different heights at the back of one of the scrapers, directed to the next scraper at an angle of 45°.

The dye solution was injected from the top through rubber tubes going down inside the shaft until the scraper height. The three rubber tubes were connected to metal tubes coming out of the shaft at three different heights from the bottom at the rear of the scraper. The flow pattern behind this scraper and in front of the next scraper was recorded during rotation by a digital camera Canon IS Powershot attached to the shaft and rotating at the same speed. In this way we were able to see the flow around the scraper blades in a reference frame revolving with the scraper. To achieve a stable light intensity, the tank was illuminated with a light projector and unwanted reflections were maximally eliminated by the use of crossed polarizers in front of the camera and the light projector.

2.3. Particle visualization

For particle visualization the same setup was used as for flow visualization but without the tubes for dye injection. The particles were $MgSO_4 \cdot 7H_2O$ crystals, with a density of 1680 kg m^{-3}, and a size distribution ranging from 0.5 to 2 mm, to mimic the situation as happens during crystallization. The particles were released at the bottom of the crystallizer and were subsequently agitated and lifted by the action of the scraper. The particles were recorded by the rotating camera following the rotating scraper. The same light conditions were used as in the dye experiments.

2.4. Computational techniques

2.4.1. Calculation of velocity fields

For the single-phase flow an in-house developed lattice-Boltzmann (LB) code has been applied. The efficiency of the LB

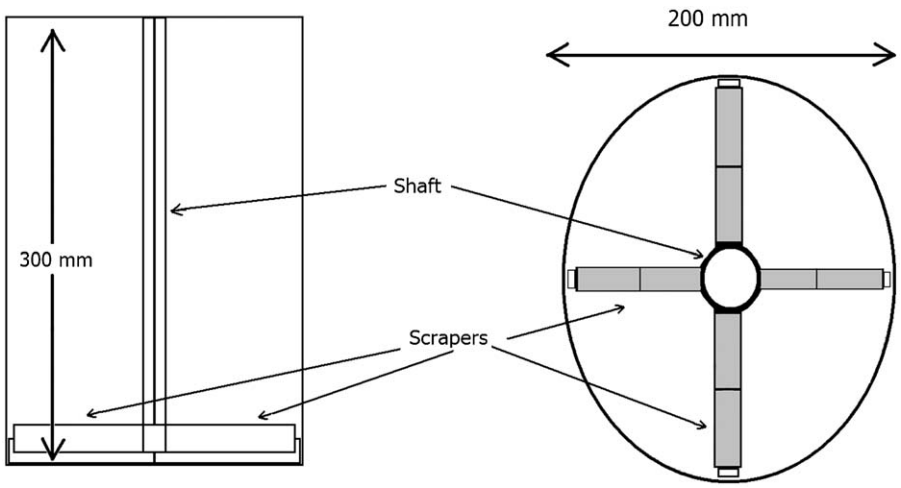

Fig. 1. Schematic drawing of the ice scaling crystallizer.

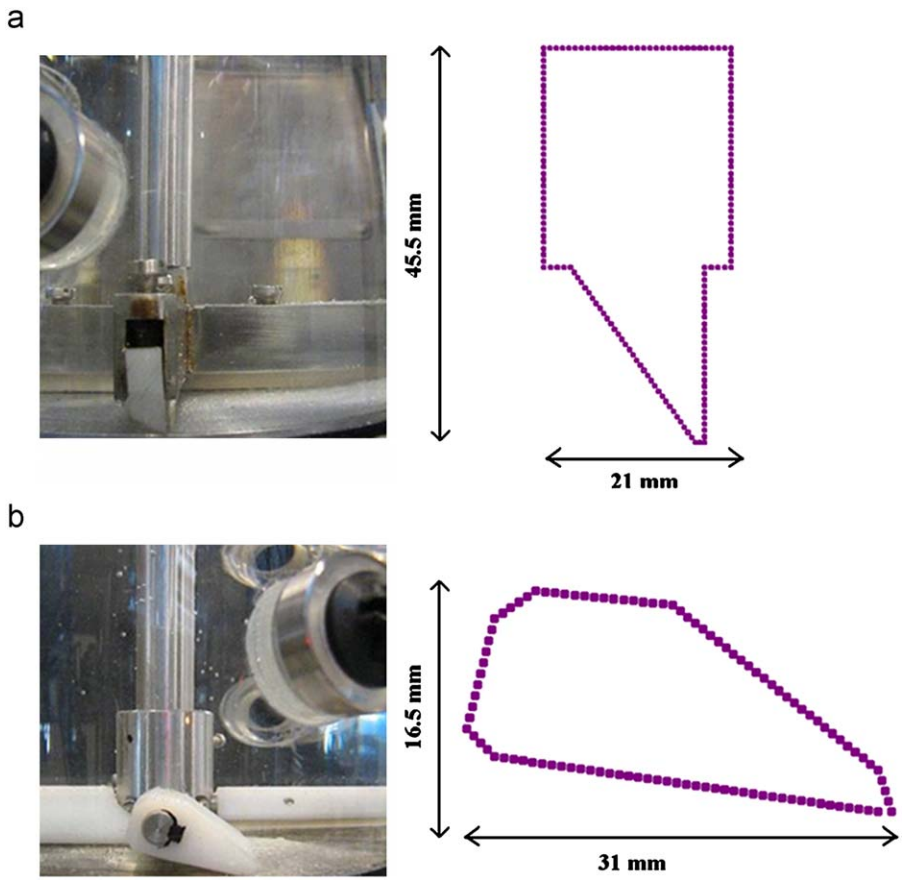

Fig. 2. The top two figures are the vertical scraper design used in the experimental crystallizer (left) and the schematic cross area of the geometry used in the CFD simulations (right). (b) The bottom two figures relate to the streamlined scraper design.

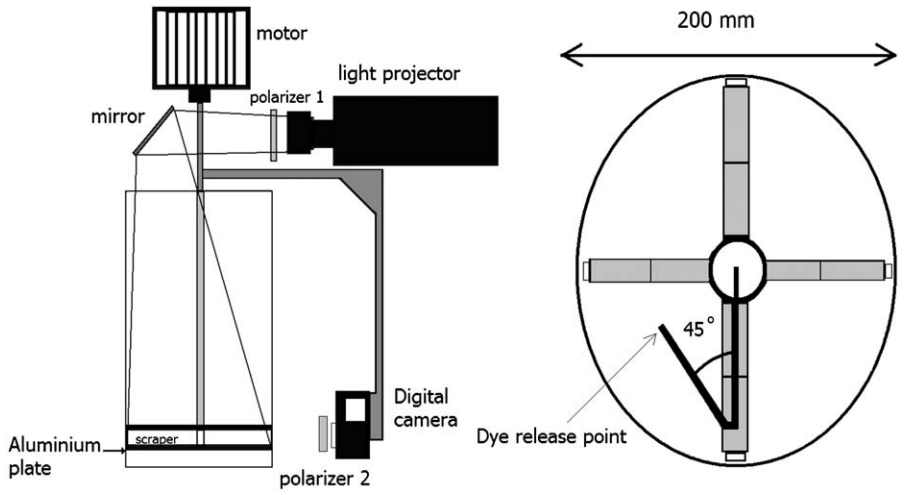

Fig. 3. Schematic setup for flow and particle visualizations (left). The picture at the right shows in black the tube for the dye injection with the angle of 45°.

method for computational fluid dynamics simulations has been shown by Somers (1993). The LB-based fluid flow code has been extended with a procedure to track solid particles through the flow domain (Euler–Lagrange approach, see also Derksen (2003)). Here, we employ the same Euler–Lagrange approach to simulate the combined fluid and particle flow in the scraping area of heat exchanger surfaces.

In order to fully resolve the flow and the particle motion (direct numerical simulations) we cannot simulate the entire crystallizer volume; we have schematized the situation as occurring in the vicinity of the HE surface and the scrapers by considering a rectangular domain of 4×10^6 grid cells ($nx = 100$, $ny = 200$, $nz = 200$) as shown in Fig. 4.

The Navier–Stokes equations are solved without the use of a turbulence model. Every grid cell corresponds to 1 mm in each direction. As boundary conditions the domain walls are made periodic in their x and y directions and for the bottom plane (scraped surface) a no-slip condition is applied. The scraper extends from one

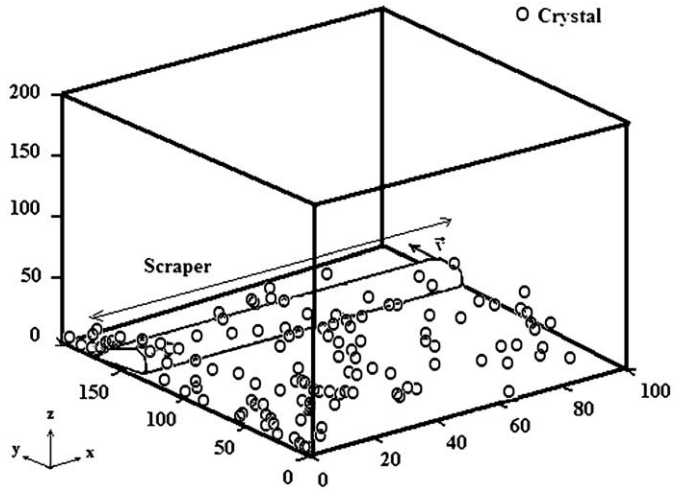

Fig. 4. Entire Computational domain with a linearly moving scraper (in the positive y direction) and crystals represented by the circles.

side of the box to the other in the x direction and moves in the y direction. Since a periodic boundary condition was applied in the y direction, we mimic the scraper meeting its own back flow as if this flow were produced by the scraper in front as happens during rotation. For the top plane of the computational domain a free slip condition is applied. The particles that arrive there are not taken into account anymore just as if they left the scraping area to the bulk and do not come back. The Reynolds number is defined as $Re = V \cdot L/\upsilon$, with V the scraper speed, L the scraper height and υ the kinematic viscosity of the working fluid. In this case we studied the Reynolds number was set to $Re = 2.5{\times}10^4$, which makes the flow turbulent. The continuous phase was water with a density $= 10^3\,\mathrm{kg\,m^{-3}}$ and viscosity $= 10^{-6}\,\mathrm{m^2\,s^{-1}}$. For the simulations the two scraper geometries as described in the experimental section were used.

As already mentioned, the simulations were performed in a linearly moving system instead of in a rotating system as were the experimental visualizations. Thus we leave out the effects of coriolis forces in the fluid flow and the centrifugal and coriolis forces on the particles (given their density difference with the liquid). These effects could have been incorporated in the simulations by adding a body force to the fluid flow equations, and additional forces acting on the particles. In this qualitative stage of research it was decided to focus on flow structures and leave refinements for future work. In terms of the particle flow around the scraper, we do not expect much effect of the centrifugal force since it would act in the x direction, whereas we observe the flow past the scraper in the yz plane (see Fig. 4).

2.4.2. Calculation of particle trajectories

The particle trajectories were calculated in a Lagrangian framework. A simple approach was undertaken in which we restricted the forces acting on the spherical particles with diameter d_p to inertia, gravity and drag forces. The equation of motion used was

$$\frac{\pi}{6}d_p^3\rho_p\frac{d\vec{v}_p}{dt} = \frac{\pi}{8}d_p^2\rho_l C_D|\vec{u}-\vec{v}_P|(\vec{u}-\vec{v}_P) + \frac{\pi}{6}d_p^3(\rho_p-\rho_l)\vec{g} \quad (1)$$

$$\frac{d\vec{x}_p}{dt} = \vec{v}_p \quad (2)$$

The velocity vector **u** of the fluid at the particle position is calculated by tri-linear interpolation of the surrounding grid velocities. For the drag coefficient we took the Schiller and Naumann (1935) correlation:

$$C_D = \frac{24}{\mathrm{Re}_p}(1.0 + 0.15\mathrm{Re}_p^{0.687}) \quad \mathrm{Re}_p < 1000 \quad (3)$$

and

$$C_D = 0.44 \quad \mathrm{Re}_p \geq 1000 \quad (4)$$

where

$$\mathrm{Re}_p = |u - v_p|\frac{d_p}{v} \quad (5)$$

The system of equations were numerically solved using semi-implicit Euler time stepping.

For easy visualization only 200 particles were released at the bottom of the flow domain in front of the scraper. They were treated as spherical particles of $d_p = 1$ mm diameter and had the density of $MgSO_4 \cdot 7H_2O$ crystals as in the experimental part. The Stokes number (defined as $St = (\rho_p/\rho_l)(d_p^2 V/vL)$) for these particles is around 3 (larger than 1) that implies they have sufficient inertia to collide with the scraper and bottom wall. The collisions with the scraper and the bottom were taken to be elastic. This means that for particle collisions with the bottom the velocity component in the z direction of the particle changes from v_p to $-v_p$, leaving the x and y components as before the collision. The final direction of particle collisions with the scraper depends on the inclination angle of the wall and the incident angle of the particle. The outgoing particle angles after colliding with the scraper only vary in the yz plane, the velocity in x direction does not change after the collision. Since the scraper is moving in the y direction, collisions with the scraper add momentum to the particles in the y direction

2.4.3. Calculation of particle–particle interactions

The method for detecting and handling particle–particle collisions was similar to the one proposed by Chen et al. (1998). In their method, they make use of a collision detection algorithm that anticipates collisions in the upcoming time step. Subsequently, the path of two particles that are bound to collide is integrated in a three-step-process: the pre-collision step, the collision step (in which the particles exchange momentum), and the post-collision step. In order to limit the computational effort spent in handling the particle–particle collisions (which in principle is an M^2 process, with M the number of particles), we have grouped the particles in each other's vicinity in a so-called link-list (Chen et al., 1998). The extent of the vicinity of a particle in which potential collision partners are sought is the lattice cell in which the particle under consideration resides, and the 26 neighbouring cells. This reduces the number of possible collisions partners to a few for a specific particle during a specific time-step.

The collision algorithm assumes that one particle can only collide once during one time step. The reason is purely practical: taking into account multiple collisions in one time step would lengthen the computations to an unfeasible extent. The assumption either limits the time step, or the particle volume fraction. In any case, in the simulations there is a finite chance that the collision detection algorithm misses a collision. This is reflected in the situation that at the next time step, two approaching particles have a mutual distance less than d_p. If this occurs, a so-called missed collision procedure is executed: directly at the start of the time-step, the particles involved are given their post-collision velocities (making that they now are moving apart). During the time step, the particles are displaced as a pair according to their average velocity, and they move apart with their relative velocity until they have a mutual separation of at least d_p.

3. Results and discussion

3.1. Streamlined scraper geometry

The results for the streamlined scraper geometry will be treated first. The experimentally obtained flow visualization results of the injected dye and the DNS calculations are presented in the rotating reference frame moving with the scraper (Fig. 5). The top two figures correspond to 20 s after start-up, and the bottom figures to 230 s. By that time the system has reached a quasi-steady state. The experimental data and DNS calculations of the flow field agree qualitatively well. Both types of results show the development of a turbulent flow with initially a well-defined eddy structure in the wake of the scraper, and a highly turbulent wake in the later stages. The initial vortex transports liquid removed from the HE surface by the front of the scraper back to the HE surface in its wake. Also after the initial vortex has dissipated, the dye visualization experiments show that fluid is hardly transported towards the bulk of the crystallizer. As a consequence, we expect the heat transfer not to be greatly enhanced by the action of the scraper: the fluid removed from the heat exchanger plate remains in the same scraping area and does not mix with the rest of the bulk solution.

For this scraper the calculation of the particle trajectories did not include particle–particle collisions. We could afford neglecting particle–particle collisions since we had a small overall solids volume fraction, and the visualization showed that there were no places where particles preferentially concentrate. The calculated particle trajectories show good agreement with the measured trajectories as can be seen in Fig. 6. At start-up the scraped particles smoothly follow the surface of the scraper and the eddy created behind the scraper returns the particles to the heat exchanger surface at the back of the scraper. As time passes the coherence of the wake eddy gets weaker and the particles are more uniformly distributed in the solution. Still many particles eventually land at the HE surface behind the scraper. During crystallization these particles will have a reseeding effect on the just cleaned surface. The benefits of having a streamlined scraper also become apparent from the visualizations and simulations. The liquid flow has relatively smooth streamlines so that the particles easily follow the flow and do not build-up in front of the scraper.

3.2. Vertical scraper geometry

For the vertical scraper geometry two different types of flow visualization experiments were done, one type where the dye was injected from the backside of the scraper moving in front of the one viewed by the digital camera (Fig. 7), and another type where the dye was released at the heat exchanger surface in front of the vertical scraper blade before the start of rotation (Fig. 8).

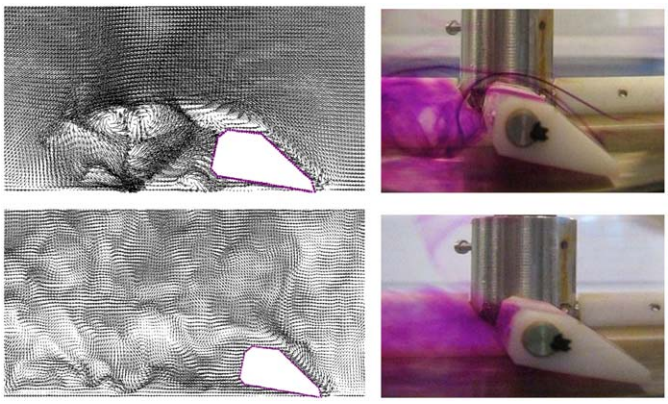

Fig. 5. Vector plane representing the velocity flow field for the streamlined scraper geometry compared to measured flow visualization. The top two figures correspond to 20 s after start-up, and the bottom two after 230 s (quasi-steady state).

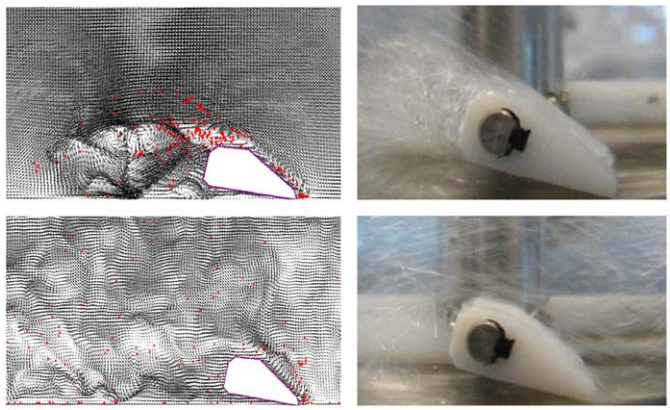

Fig. 6. Particle trajectories from particle-flow simulations for the streamlined scraper geometry compared to measured particle-flow visualization. The top two figures correspond to 20 s after start-up, and the bottom two after 230 s after reaching a quasi-steady state.

From the pattern of the dye released from the back of the scraper in front of the one observed by the camera, it can be observed that the fluid in front of the scraper is pushed forward by the approaching scraper wall and then is thrown upwards along the scraper wall and beyond (i.e. higher up in the tank). Eventually the dye is being sucked down again (Fig. 7).

From the pattern of the dye released just above the heat exchanger surface it can be observed that the dye partly climbs upwards against the approaching scraper wall and then moves over the top of the scraper. The other part of the dye ascends much further away in front of the scraper (Fig. 8). This rising flow far from the front wall of the scraper is the consequence of the eddy formed behind each scraper that pushes dye from the scraped surface upwards. These two upwardly directed flows meet and create the triangular area free of dye observed just above the vertical scraper in the right picture of Fig. 8.

The observations from the dye patterns are qualitatively in agreement with the DNS results presented in Fig. 9. An instantaneous shot of the calculated flow pattern of the vertical scraper is shown in Fig. 9. It is clearly visible how close to the front of the vertical scraper wall the liquid is pushed upwards and that an eddy is created behind the scraper with a linear size roughly twice the scraper height. This eddy transports the fluid that passes over the top of the scraper down to the surface and rolls it upwards again more closely behind the scraper; the two up flows meet and create the triangular cone free of dye above the scraper that was shown in Fig. 8.

The particle visualizations of the vertical scraper show that initially the particles are piled up against the front wall of the vertical scraper forming a triangular particle build-up region at the tip of the scraper. After this building up the particles start to get pushed up by the upward flow in front of the scraper (Fig. 10).

When this process is followed in time (Fig. 11) a triangular area of piled up particles is created in front of the scraper, and the newly arriving particles are pushed over the top of the scraper by the flow.

In simulating particle trajectories, initially we neglected the effects of particle–particle collisions on the motion of the particles, just as we did with the streamlined scraper. As initial condition, all particles are positioned upon the scraped surface in front of the scraper (as in the experiments). The computational results differ from the real situation because no piling up of particles in front of

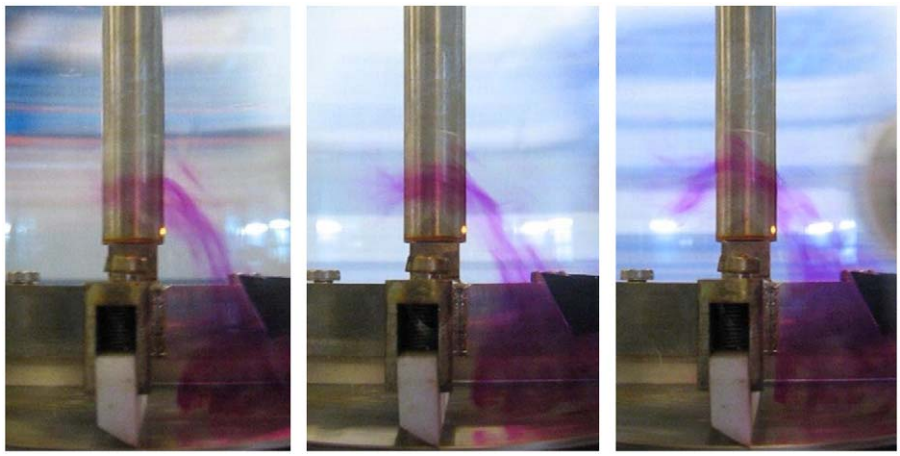

Fig. 7. Snapshots of the flow visualization with dye injected at the back of scraper in front of the scraper observed; vertical scraper geometry. The time between frames is 5×10^{-2} s.

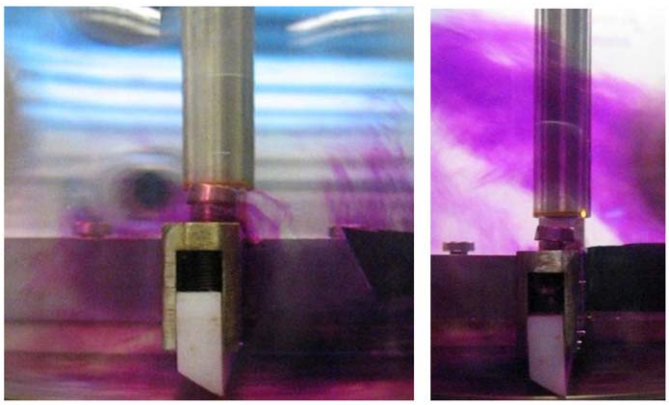

Fig. 8. Snapshots from dye released above the bottom during the starting up. The time between frames is 5×10^{-1} s.

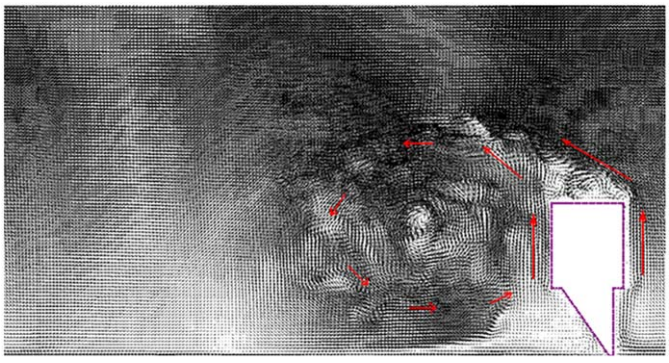

Fig. 9. Instantaneous velocity flow field of the vertical scraper geometry in the reference frame of the moving scraper at 2×10^{-1} s after starting up.

Fig. 10. Snapshot of $MgSO_4 \cdot 7H_2O$ crystals scraped from the heat exchanger surface at 7×10^{-1} s after starting up. In front and at the bottom of the scraper a triangular build-up of particles is formed.

the scraper occurs as can be seen from Fig. 12. This is so because if no particle–particle collisions are taken into account, the particles can occupy the same space. Also particle–fluid coupling has not been applied and the fluid flow field does not feel the presence of the particles.

Before implementing particle-particle collisions in the simulation code we first wanted to confirm that the absence of particle build-up in front of the scraper was responsible for the difference between particle behavior in simulation and experiment. To do this we created an artificial build-up volume by extending the scraper with a triangular region (see Fig. 13). The size of the triangle was based on our experimental observations

Once this artificial build-up is added to the scraper shape the simulations of the particles properly reflect the measured situation as shown in Fig. 10.

The locally high solids volume fractions in front of the vertical scraper clearly demonstrated the need for considering particle–particle collisions when integrating the motion of the particles.

Therefore our simulation procedure without the additional triangular extension was extended with (fully elastic) particle–particle collisions to mimic realistically the particle trajectories. In Fig. 14 it is shown how a simulation with 2000 particles properly creates a build-up, just as in the particle visualization experiments.

To better visualize the flow and its influence on the particle trajectories the number of particles was restricted to 200 in the visualization (though kept to 2000 in the simulations). Five snapshots of the simulations at time intervals of 2.5×10^{-2} s (from 2×10^{-1} s after start) are given in Fig. 15.

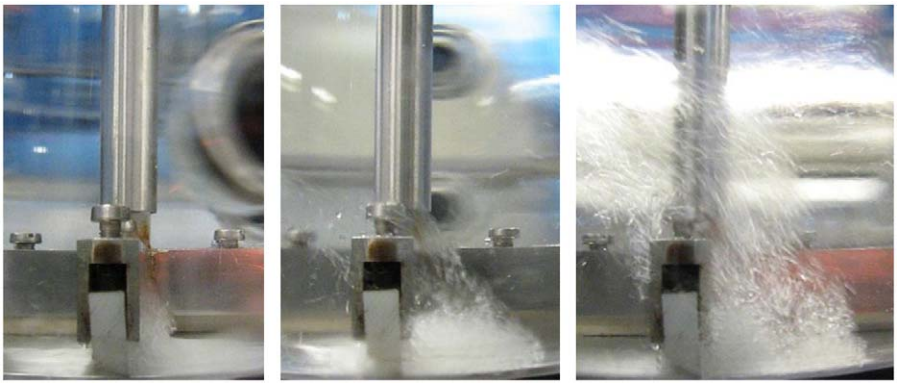

Fig. 11. Snapshots of the $MgSO_4 \cdot 7H_2O$ crystal particles scraped from the heat exchanger surface during start-up behaviour. The time spacing between the frames is 5×10^{-2} s.

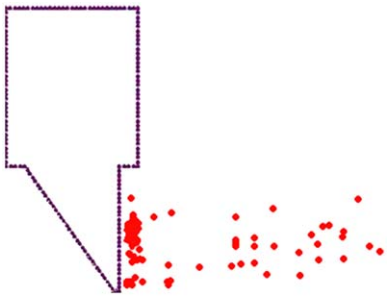

Fig. 12. Image of the computational simulations that show piling up of particles (red dots) at the bottom of the vertical scraper at 7×10^{-1} s after starting up. (Note: The particles are depicted irrespective from their x coordinate.) (For interpretation of the references to colour in this figure legend, the reader is referred to the web version of this article.)

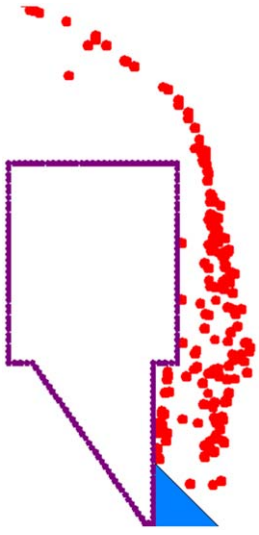

Fig. 13. Vertical scraper geometry (green) with the artificial particle build-up in front of the scraper (blue) at 7×10^{-1} s after starting up. (For interpretation of the references to colour in this figure legend, the reader is referred to the web version of this article.)

In the second frame of Fig. 15 the particles start passing over the scraper and are carried to the top of the main eddy that is created in the wake of the scraper when starting it up. This eddy gradually disintegrates into smaller eddies and turbulent structures.

In the third frame the start-up eddy approaches the front of the next scraper, causing a downward oriented flow there. This downward flow passes through the particles that have reached the top of the vertical scraper, and pulls them down again towards the HE surface in front of the scraper. Also some particles that are already above the top of the scraper are transported horizontally by this turbulent flow a further distance in front of the scraper. The same situation is visible in the second frame of Fig. 11. The last two frames of Fig. 15 show how the eddy keeps approaching the scraper while carrying the particles. It finally disintegrates by interacting with the front of the scraper leaving behind a turbulent field. When this occurs the flow field in front of the scraper carries the particles from a wide region in front of the scraper upwards to the bulk, in agreement with the visualization results presented in the third frame of Fig. 11.

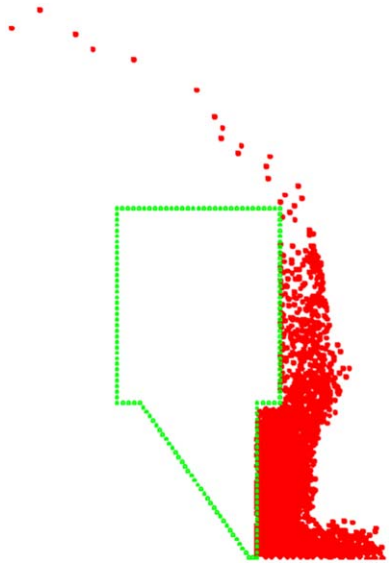

Fig. 14. Simulation of 2000 particles scraped from the bottom surface at 7×10^{-1} s after starting up.

The simulations show that neither the streamlined scraper nor the vertical scraper was good scraper designs. The streamlined scraper because it does not mix the scraped thermal boundary layer with the bulk solution and redirects the scraped particles to the clean surface in the wake of the scraper. The vertical scraper is inadequate because it accumulates the particles in front of the scraper, but the mixing of the thermal layer with the bulk solution is better. An improvement of the vertical scraper could be the triangular addition to the bottom part of the vertical wall of the scraper to avoid the appearance of the front build-up.

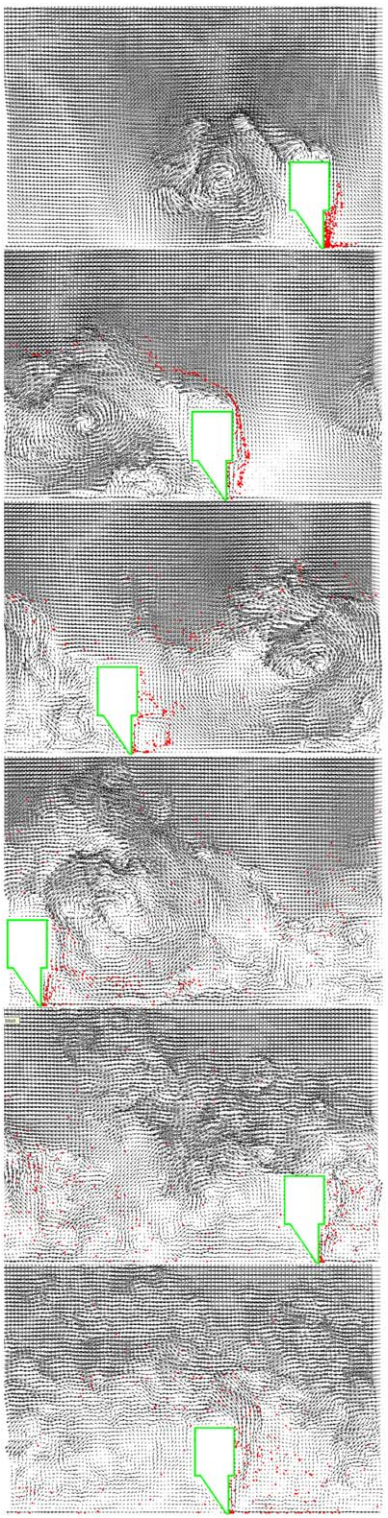

Fig. 15. Snapshots of the particle-flow simulations at time intervals of 2.5×10^{-2} s.

4. Conclusions

We studied the flow and solid particle trajectories induced by a scraper moving over a flat wall, mimicking the heat exchanging surface in freeze crystallization. The focal point of research was the impact the scraper geometry has on parameters influencing the stability of the crystallization process such as scraping efficiency, mixing of solute and crystals, and directing scraped-off crystals towards the bulk of the crystallizer. Two specific scraper geometries were compared in this respect. An approach based on experimental flow and particle visualization was combined with direct numerical simulations. The particle-flow simulations used lattice-Boltzmann discretization to solve the Navier–Stokes equations, and a Lagrangian approach to particle tracking.

The simulation results were in qualitative agreement with the experimental visualizations of the same system. In this first attempt to simulate the particle and flow behaviour we made a couple of simplifying assumptions: with respect to particle motion only drag and gravity forces acting on the particles were taken into account. Furthermore particles collided elastically with the HE surface and the walls defining the moving scraper. Since we considered relatively low particle loadings, we initially neglected two-way coupling between liquid and particles, and particle–particle collisions. The latter neglect proved critical for one of the scrapers where a build-up of particles was observed experimentally. Also, the simulations were done with a linearly translating scraper through a periodic domain, whereas in the experiment the scraper is revolving. Given the qualitative agreement between simulations and experiments the absence of centrifugal and coriolis forces was not felt strongly. Adding body forces induced by rotation to the simulation procedure is very well doable and will be considered in future work.

Our numerical approach without particle–particle collisions provided satisfactory results for the streamlined scraper because this shape did not accumulate the particles during its scraper action. For the vertically oriented scraper this simulation approach failed due to the build-up of particles as could be observed from the visualisation experiments. It was therefore considered to be essential to include particle–particle collisions in order to predict accumulation of particles. When this was implemented the simulations were in agreement with the results of the visualization experiments.

The simulations provided good insight in the behaviour of the particles and the fluid flow induced by the two scraper geometries. In case of the streamlined scraper the particles smoothly follow the flow that transports them over the top of the scraper, but are redirected to the surface at the back of the scraper. Also due to its shape the thermal layer removed from the scraped heat exchanger surface remains close to the scraping area and does not strongly mix with the bulk fluid which does not enhance heat transfer as much as one would wish. In contrast, a vertically oriented scraper mixes the removed thermal layer higher up with the bulk. The downside of the vertically oriented scraper is a strong build-up of particles at its front. This may contribute in insulating the HE surface from its surroundings, and in forming bigger chunks of (ice) crystals when the build-up agglomerates. These big agglomerates being released in the crystallizer form a serious risk for the stability of the process. In the paper we suggest that this situation could be avoided by adding a scup at the front wall of the scraper.

In a broader sense, we strongly believe that detailed numerical simulations contribute to improving scraper design for more efficient and stable cooling crystallization processes.

References

Chen, M., Kontomaris, K., Mc Laughlin, J.B., 1998. Direct numerical simulation of droplet collisions in a turbulent channel flow. Part I: collision algorithm. International Journal of Multiphase Flow 24, 1079–1103.

De Goede, R., De Jong, E.J., 1993. Heat transfer properties of a scraped-surface heat exchanger in the turbulent flow regime. Chemical Engineering Science 48 (8), 1393–1404.

Derksen, J.J., 2003. Numerical simulation of solids suspension in a stirred tank. A.I.Ch.E. Journal 49, 2700.

Duffy, B.R., Wilson, S.K., Lee, M.E.M., 2007. A mathematical model of fluid flow in a scraped-surface heat exchanger. Journal of Engineering Mathematics 57 (4), 381–405.

Fitt, A.D., Please, C.P., 2001. Asymptotic analysis of the flow of shear-thinning foodstuffs in annular scraped heat exchangers. Journal of Engineering Mathematics 39 (1–4), 345–366.

Landfeld, A., Kyhos, K., Strohalm, J., Sestak, J., Houska, M., 2006. Heat transfer with heating and cooling granular materials in a scraped-surface homogeniser. Journal of Food Engineering 77 (3), 708–712.

Pronk, P., Infante-Ferreira, C.A., Rodriguez Pascual, M., Witkamp, G.J., 2005. Maximum temperature difference without ice scaling in a scraped heat exchanger crystallizer. In: Proceedings of the 16th International Symposium on Industrial Crystallization, pp. 1141–1146.

Pronk, P., Infante Ferreira, C.A., Witkamp, G.J., 2008. Prevention of crystallization fouling during eutectic freeze crystallization in fluidized bed heat exchangers. Chemical Engineering and Processing: Process Intensification 47 (12), 2140–2149.

Qin, F., Chen, X.D., Ramachandra, S., Free, K., 2006. Heat transfer and power consumption in a scraped-surface heat exchanger while freezing aqueous solutions. Separation and Purification Technology 48 (2), 150–158.

Rao, C.S., Hartel, R.W., 2006. Scraped surface heat exchangers. Separation and Purification Technology 48 (2), 150–158.

Rodriguez Pascual, M., Ravelet, F., Delfos, R., Witkamp, G.J., 2009. Large eddy simulations and stereoscopic particle image velocimetry measurements in a scraped heat exchanger crystallizer geometry. Chemical Engineering Science 64 (9), 2127–2135.

Schiller, L., Naumann, Z., 1935. A drag coefficient correlation. Zeitschrift des Vereines Deutscher Ingenieure, 77–318.

Stranzinger, M., Bieder, A., Feigl, K., Windhab, E., 2002. Effects of flow incidence and secondary mass flow rate on flow structuring contributions in scraped surface heat exchangers. Journal of Food Process Engineering 25 (3), 159–187.

Somers, J.A., 1993. Direct simulations of fluid flow with cellular automata and the lattice-Boltzmann equation. Applied Science Research 51, 127.

Vaessen, R.J.C., Seckler, M.M., Witkamp, G.J., 2004. Heat transfer in scraped eutectic crystallizers. International Journal of Heat and Mass Transfer 47 (4), 717–728.

Yataghene, M., Pruvost, J., Fayolle, F., Legrand, J., 2008. CFD analysis of the flow pattern and local shear rate in a scraped surface heat exchanger. Chemical Engineering and Processing: Process Intensification 47 (9–10), 1550–1561.